Rüther, U., Koenen, M., Otto, K., & Müller-Hill, B. (1981) *Nucleic Acids Res. 9*, 4087–4097.
Shapira, S. K., Chou, J., Richaud, F. V., & Casadaban, M. J. (1983) *Gene 25*, 71–82.
Srere, P. A., & Mosbach, K. (1974) *Annu. Rev. Microbiol. 28*, 61–83.
Srere, P. A., Mattiasson, B., & Mosbach, K. (1973) *Proc. Natl. Acad. Sci. U.S.A. 70*, 2534–2538.
Welch, G. R., Ed. (1985) in *Organized Multienzyme Systems*, Academic Press, New York.
Zalkin, H., Paluh, J. L., van Cleemput, M., Moye, W., & Yanofsky, C. (1984) *J. Biol. Chem. 259*, 3985–3992.

A Dynamic Model for the Structure of Acyl Carrier Protein in Solution†

Yangmee Kim and J. H. Prestegard*
Department of Chemistry, Yale University, New Haven, Connecticut 06511
Received January 19, 1989; Revised Manuscript Received July 6, 1989

ABSTRACT: The determination of solution structures of proteins using two-dimensional NMR data is commonly based on the assumption that the structure can be represented by a single rigid conformer. We present here a procedure whereby this assumption can be relaxed and illustrate its application to acyl carrier protein from *Escherichia coli*, a small negatively charged protein with no internal disulfide bonds. The methodology rests on a model having two distinct conformers in dynamic equilibrium. Use of this two-state model results in a dramatic improvement in fit to cross-relaxation-derived distance constraints and a substantial lowering of molecular mechanics energies for individual conformers of acyl carrier protein. The two-state model retains the three-helix motif previously identified on the basis of a one-state structure, but substantial motion of loop regions and the C-terminal peptide, as well as partial disruption of the second helix, is suggested to occur. Support for the existence of these motions can be found in amide exchange rate and spin relaxation time data.

Recent advances in NMR instrumentation and methodology have made it possible to acquire sufficient distance constraints from proton–proton nuclear Overhauser effects (NOEs)[1] to attempt determination of the structures of small proteins in solution (Braun et al., 1983; Havel & Wuthrich, 1985; Clore et al., 1987a; Holak et al., 1988a; Moore et al., 1988). A number of examples of successful application now exist including ones showing excellent agreement of X-ray and NMR structures (Clore et al., 1986, 1987a; Wagner et al., 1987; Kline et al., 1988).

The protocols developed for converting NOE measurements into structures vary widely (Braun & Go, 1985; Clore et al., 1985, 1987b; Wagner et al., 1987; Holak et al., 1988a; Kline et al., 1988). However, most employ a $1/r^6$ interproton distance dependence of NOEs—a relationship that stems from an assumption that protons are rigidly fixed in a well-defined protein structure and that proton–proton dipolar interactions are modulated by a single isotropic molecular tumbling motion. Violation of this assumption by the presence of some types of motion, for example, the presence of rapid, uncorrelated internal motions, will have small effects on derived structures (LeMaster et al., 1988). However, one would expect more severe effects due to the presence of slower internal motions. Recognition of possible violations of assumptions underlying a straightforward conversion of NOE intensities to distances is, in part, reflected in the reluctance of many authors to do more than set, upper and lower bounds, for NOE-based distances (Braun & Go, 1985; Clore et al., 1987b; Wagner et al., 1987). It is possible, however, to employ a more precise distance specification if one explicitly allows for the presence of slow internal motions in deriving a structure. We hope to illustrate this point, with an application to acyl carrier protein from *Escherichia coli* (ACP).

ACP is typical of many proteins studied by NMR in terms of its size, 8847 daltons, and in terms of the quality of NMR data obtained. ACP differs, however, from many proteins studied in that it has no intramolecular disulfide bonds to stabilize a single well-defined structure (Wagner et al., 1987) and in that it may be further destabilized by a high net negative charge (−16 at pH 5.9). It is a protein in which one might expect effects of motion to be pronounced.

The structure of ACP has been determined without explicit treatment of motion, using both a simulated annealing approach, which employs upper and lower bounds for distances (Holak et al., 1988b), and a molecular mechanics pseudoenergy approach, which employs a single best estimate of interproton distances (Holak et al., 1988a). The quality of these structures is often assessed on the basis of convergence of solutions from multiple starting points to a single structure, and on the basis of divergence of interproton distances in the final structures from experimental constraints. The structure produced by simulated annealing looks good on both of these counts. The average RMS deviation of backbone atoms from their mean position is 2 Å, and the number of distance violations greater than 0.5 Å for the average structure is very small. A refinement published during preparation of this paper, in fact, finds a much smaller RMS deviation of back-

† Supported by a research grant from the National Institutes of Health (GM32243).

[1] Abbreviations: NOE, nuclear Overhauser effect; ACP, acyl carrier protein; RMS, root mean square; AMBER, assisted model building with energy refinement.

0006-2960/89/0428-8792$01.50/0

bone atoms and no distance deviations larger than 0.5 Å (Holak et al., 1989). The structure produced from the pseudoenergy structure does not, on the surface, appear to be as good. RMS deviations of backbone atoms from the average structure range from 2.0 to 3.0 Å, and RMS deviations of distances between protons found in the structures and the corresponding experimental distances range from 0.5 to 0.86 Å for distances determined from NOEs with no ambiguity in their assignment or volume integration. It is, however, difficult to compare these numbers. Deviations in distances in the first case are from the upper and lower bound limits and not the best estimate of the distance. For direct comparison, something on the order of half a typical difference between upper and lower bounds should be added to the distance violations in the simulated annealing calculation. Also, the constraint function in the simulated annealing calculation, which is a modified square well, will not allow large deviations among structures. The pseudoenergy function employed in the molecular mechanics approach imposes only a small finite penalty for deviations to the large side and allows much greater divergence among structures.

In some cases, the large divergences which result in the pseudoenergy–molecular mechanics approach are useful in highlighting areas of the molecule which have conflicting distance constraints as derived on the basis of a single rigid model for the molecule. Phe-50, for example, is observed to have short distance constraints involving Ile-3, Leu-46, and Ile-72. All structures violate one or more of these constraints by having a distance which is too long. While it is possible that violation results from the failure of the structure determination algorithm to find an appropriate structure, the observation of abnormally short constraints to distant sites is precisely the type of artifact expected from averaging of NOEs over two or more discrete structures. In this paper, we present support for the existence of motional averaging in ACP by fitting NOE data to a simple two-state model.

Materials and Methods

If we assume that multiple conformations interchange on time scales shorter than the cross-relaxation time, but longer than the time which characterizes molecular tumbling, the measured cross-relaxation rate leading to an observed NOE intensity is a simple average of rates which exist for each conformer. Therefore, the average relaxation rate for a pair of protons, a and b, exchanging between two conformational states can be expressed as

$$\sigma_{ab} = \chi_1\sigma_{1ab} + (1 - \chi_1)\sigma_{2ab} \quad (1)$$

where χ_1 is the mole fraction of the first conformation and σ_{1ab} and σ_{2ab} are the cross-relaxation rates in conformations 1 and 2, respectively. σ_{1ab} and σ_{2ab} can be calculated from the atomic coordinates of any two conformers and combined by using expression 1 for comparison to the experimentally observed cross-relaxation rate σ_{oab}. Ideally, one would manipulate conformations to minimize deviations between σ_{ab} and σ_{oab}. In doing this, one must, however, have regard for molecular bonding and nonbonding constraints as well as NMR-derived constraints. To ensure that we treat each adequately, we define a function which combines molecular constraints and NMR distance constraints in the form of a total energy function which can be minimized. The total energy, E, is the sum of the molecular energies of the two conformations, E_1 and E_2, and a pseudoenergy, E_{NOE}, for each observed NOE:

$$E = E_1 + E_2 + \sum_{a>b} E_{NOE}(\sigma_{ab}) \quad (2)$$

The pseudoenergy term is given by

$$E_{NOE} = W(\sqrt{\sigma_{ab}} - \sqrt{\sigma_{oab}})^2 \quad (3)$$

where W is a weighting factor[2] chosen to allow reasonable interplay of molecular and NMR energies. The molecular energies are calculated by using the program AMBER[3] with the united atom force field, and the combined energies are minimized within the framework of AMBER following a protocol described in previous works (Holak et al., 1988a).

The mole fraction of each conformer, χ_i, could, in principle, be calculated by using a Boltzmann factor and the molecular energy of each conformer, E_1 and E_2 (Scarsdale et al., 1988). Use of such factors, however, demands extreme accuracy in calculated energies. While we regard energies calculated by AMBER as a good basis for rejecting structures which have unreasonably high molecular energies, they are not sufficiently accurate to dictate fractional populations.

An alternative to the use of Boltzmann factors involves adjusting χ_i to optimize fit to experimental data for a fixed pair of conformations. This procedure would assume the conformations chosen to be reasonably close to the actual conformations involved in averaging. Our most reasonable source of conformers is the set of seven solutions generated by using a single conformer assumption (Holak et al., 1988a). It is not obvious that members of this set would approximate individual contributors to an average. Most protocols used in the literature would not, in fact, yield a good approximation of individual conformers, because superposition of conflicting constraints represented by square or harmonic pseudoenergy functions frequently leads to a single compromise minimum in the potential energy surface. The highly asymmetric pseudoenergy function used with the molecular mechanics approach to generate the single conformer set for ACP, however, has the unusual property of generating multiple minima when conflicting constraints are superimposed. Structures determined tend to fall in one minimum or another and are in many cases reasonable approximations of individual averaging structures. For example, in the limit that the two structures are equally populated, the distance error introduced in assuming an NOE to come from one structure is on the order of $2^{1/6}$, or a factor of 1.12. A structure satisfying even this incorrectly interpreted data will, therefore, be very close to the actual structure.

Hence, we will use pairs of one state solutions to calculate mole fractions which give an optimum fit to NOE data and then optimize structural coordinates at a fixed values of χ_i. This procedure could be applied iteratively, but this is a computationally intensive process. To further improve the fit to data, energy minimization was carried out by using AMBER and a three-step protocol described in our earlier paper (Holak et al., 1988a). The last two steps in the minimization, which represent the major time investment, were carried out on a Multiflow Trace 7 computer and require about 35 h per structure. Given this time requirement, only one iteration was employed.

Results and Discussion

Table I shows data pertaining to the four best one-state solutions for the ACP structure determined previously with the pseudoenergy–molecular mechanics approach (Holak et

[2] W is chosen so that a violation of a 3-Å constraint to the long-distance limit results in a penalty of approximately 10 kcal.

[3] AMBER 3.0 (U. C. Singh, P. K. Weiner, D. A. Case, J. Caldwell, and P. A. Kollman, 1986) is a program obtained through a licensing agreement with the Reagents of the University of California at San Francisco.

Table I: Distance Deviations and Energies for ACP Structures[a]

structure	total E	constant E	RMS[b] distance deviation	no. of distance violations[c]	distance violations involving F50, F28[d]
A	−1.56 E04	−1.80 E04	0.795	40	F50 CZ–L46 HG 4.35
					F50 HZ–L46 HA 2.48
					F28 CZ–T63 HA 2.11
B	−1.82 E04	−1.85 E04	0.503	30	F50 HZ–I03 HD 2.33
					F50 CZ–I03 HD 2.39
					F28 CZ–T63 HA 2.83
E	−1.67 E04	−1.80 E04	0.531	31	F50 CZ–I03 HD 1.38
F	−1.65 E04	−1.79 E04	0.860	40	F50 CZ–I03 HG 3.25
					F50 HZ–I03 HG 3.60
					F50 CG–I72 HG 2.93
					F50 CZ–I72 HG 2.81
					F50 HZ–I72 HG 3.48
					F50 HZ–I72 HD 4.70
					F50 CG–I72 HD 6.10
					F50 CZ–I72 HD 5.08
					F28 HZ–L42 HD2 2.21
					F28 CG–T63 HA 4.11
					F28 CZ–T63 HA 4.43

[a] Energies are given in kilocalories. Distance deviations are given in angstroms. Pseudoenergies were assigned a weighting factor of 30 kcal/mol except for cases involving overlap or use of pseudoatoms. [b] Only experimental distances of sufficient precision to justify weights of more than 10 kcal in the minimization were included. [c] Only distance deviations which are larger than 1 Å and have weights more than 10 kcal were included. [d] This connectivity information is given in terms of a one-letter code for the amino acid type followed by a sequence number and atom type. Deviations over 2 Å are reported for A, B, and F; deviations over 1.3 Å are reported for E.

Table II: Optimized Mixtures of Conformers in a Two-State Model

combination	RMS deviation	no. of distance violations >1 Å
AB (40:60)	0.398	17
AE (40:60)	0.419	18
AF (50:50)	0.480	17
BE (50:50)	0.380	13
BF (50:50)	0.419	14
EF (50:50)	0.390	14

al., 1988a). All show moderately low deviations from distance constraints and similar constraint energies, but note that each has a list of distance violations well over expected experimental precision. Those involving Phe-50 and Phe-28 are listed to illustrate the fact that each conformer violates a different set of constraints.

Optimum mole fractions for different pairwise combinations of one-state solutions conformations were determined on the basis of minimization of RMS deviations from distance constraints and minimization of the total number of distance violations over 1 Å. Table II shows data for the combinations AB, AE, AF, BE, BF, and EF determined by this method. Note that both RMS distance deviations and the number of constraint violations are reduced from the one-state models just by assuming that NOEs measured are the result of averaging. Because the two-state models AB, BE, and EF have the best RMS deviation from distance constraints and BE, BF, and EF have the smallest number of distance violations over 1 Å, the four combinations AB, BE, BF, and EF were chosen for minimization. The results are shown in Table III. Comparison between the RMS distance deviations of starting structures (Table I) and those of final structures (Table III) shows that minimization of the averaging model leads to significantly better fits of distance constraints. In the best cases, RMS distance deviations have dropped by nearly a factor of 2, and the number of distance violations over 1 Å has dropped by a factor of 3 or more. In the cases of BE and BF, no distance deviations over 2 Å are found after minimization. Also, for these combinations, molecular energies are approximately 100 kcal/mol lower than those for individual conformations, showing that energetically the two-state models are much more acceptable than the one-state models.

Table III: Distance Deviations after Minimization

combination	distance violations over 2 Å	no. of distance violations over 1 Å	RMS distance deviations	RMS atomic deviations[a]
AB (40:60)	F50 CG–L46 HA 2.154	12	0.398	2.27
	E13HN–I10 HA 2.102			
	Y71 CG–T52 HG 2.064			
BE (50:50)		5	0.284	2.19
BF (50:50)		7	0.307	1.96
EF (50:50)	F50 CZ–I72 HD 3.137	9	0.363	2.51

[a] RMS distance deviations between atoms in the two-conformation model before minimization and corresponding atoms after minimization.

The RMS deviations between starting structures and final structures are also listed in Table III. It is clear that significant changes in conformation have occurred. A good number of the changes would appear to be associated with relief of strain which had been introduced in the one-state solutions in an effort to satisfy distance constraints based on improperly interpreted NOEs. This can be seen from Ramachandran plots for the B structure backbone torsion angles as they exist in the one-state solution and in the BE combination (Figure 1A and Figure 1B, respectively). One Φ, Ψ point exists for each residue, and its symbol is chosen to represent the energy contribution for that residue (filled triangles and squares are the lowest energies). One notes that the B structure, as it exists in the two-state model (B′), has a decidedly larger number of low-energy residues (more filled symbols) and there is a tendency for Φ, Ψ combinations to converge toward areas typical of α-helical and linear peptide backbone configurations.

While the changes are substantial in terms of RMS movement of backbone atoms (2–2.5 Å), it is important to realize that this is within the range of differences among initial one-state pseudoenergy structures (Holak et al., 1988a). Except for some distortion of helical segments and displacement of a loop from residue 16 to residue 36, all structures also maintain a qualitative similarity to the average of simulated annealing structures. All have a three-helix bundle and

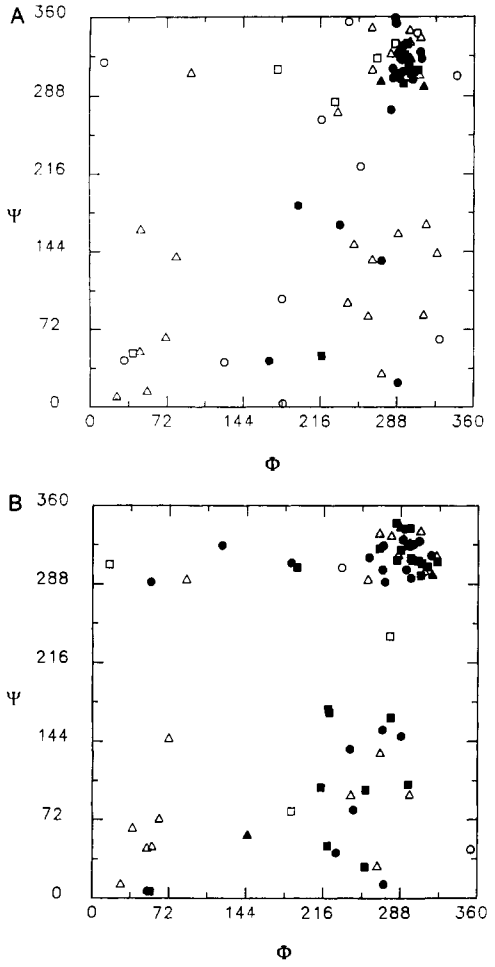

FIGURE 1: Ramachandran plots for the backbone structure of B in the one-state model (A) and the two-state model (B). Residue energies are indicated as follows: (▲) energy < −5 kcal/mol; (■) −5 ≤ energy < −2.5 kcal/mol; (●) −2.5 ≤ energy < 0 kcal/mol; (△) 0 ≤ energy < 10 kcal/mol; (□) 10 ≤ energy < 20 kcal/mol; (○) energy ≥ 20 kcal/mol.

a recognizable segment of a fourth helix (residues 56–63). The B′ structure is closest to the average simulated annealing structure with a RMS deviation of backbone atoms of 3.4 Å.

Figure 2A compares the backbone structure of the two states represented in the BE model. The poorly formed helix from residues 3 to 14 is designated as helix I, a helix from residues 37 to 51 is designated helix II, and a helix from residues 65 to 75 is designated helix III. This figure and Table IV give a picture of the motional averaging that would have to occur if this two-state model proved correct. Significant displacement of both helical and loop regions would occur, with the largest variations being in the loop regions. The motion of some side chains is shown in Figure 2B,C. Figure 2B focuses on the residues involved in the violations cited as motivation for pursuing a two-state model, namely, Phe-50, Leu-46, Ile-3, and Ile-72. Phe-50 in the B′ conformer (solid line) has close contacts with Ile-3, Leu-46, and Ile-72. Phe-50 in the E′ conformer (dashed lines) has close contacts with only Ile-3 and Leu-46. Figure 2C shows the contacts of Phe-28 with Thr-63 and Leu-42, another region with substantial side chain motion. Figure 3A shows the motional averaging for the two-state model BF. In Figure 3B, the B″ structure satisfies all Phe-50 and Phe-28 distance constraints (solid lines) while the F′ structure has close contacts of Phe-50 with only Leu-46 and Ile-3 and close contacts of Phe-28 with only Leu-42 (dashed lines). In both models, the first loop, where Phe-28 is located, moves a great deal.

Table IV: RMS Deviations of Atomic Positions in Structural Elements of One- and Two-State Models (Å)

	first helix	second helix	third helix	first loop	second loop
		B′ in BE			
E′ in BE	2.59	2.20	2.93	4.43	2.79
one-state B	1.29	0.34	0.56	1.96	0.59
		B″ in BF			
F′ in BF	4.02	2.81	0.99	4.01	2.31
one-state B	1.25	0.34	0.69	1.50	0.71
		E′ in BE			
one-state E	2.94	1.51	3.02	1.36	1.07
		F′ in BF			
one-state F	1.13	1.53	0.61	1.44	0.98

While the detailed conformations are different in the BE and BF models, there are similarities in the types of motion seen. In most cases, helices move in a concerted fashion rather than being disrupted. As shown in Table IV, in BE the third helix moves significantly, and in BF the first helix moves significantly, but both remain in similar conformations. One instance of helix disruption does occur in the second helix. The second helix of both E and F structures in one-state and two-state models is disrupted while it is a near-perfect helix in the B structure.

Despite the improvement in fit to experimental data, one must be cautious about interpreting the conformations seen in the two-state averaging models too literally. They are produced by adding an additional degree of freedom to the problem, and the assumption of two, as opposed to multiple, conformations is quite arbitrary. We can, however, cite some additional evidence in support of the types of motion we envision occurring. The disruption of the second helix, for example, should be reflected in parameters not used directly in the structure determination, such as amide proton exchange rates, along the peptide backbone. The amide protons of residues 41 and 42 do in fact exchange faster than the other amide protons in α-helices, an indication of structural instability (Englander & Kallenbach, 1983; Wagner et al., 1984). Figure 4 shows time courses of exchange of protons for deuterium at amide sites in helix II. All time courses are long compared to typical amides in loop regions, but note that amides at 41 and 42 exchange faster than amides to either side of these positions. The sites of disruption in structure E′ and F′ are not exactly at residues 41 and 42. They are closer to the center of the helix. Some evidence for disruption does, however, support the general type of motion postulated.

It is also possible to cite experimental data supporting suggested motion in other parts of the ACP molecule. Our earlier work on spin relaxation phenomena that reflect internal motion in ACP shows a higher degree of internal motion at the C terminus (Kay et al., 1988). Among all seven alanines in ACP, only Ala-77 shows evidence of internal motion other than methyl rotation. While some localized motion of the terminal residue may be expected in any case, it may also be a reflection of the more extensive motion of the C terminus seen in comparing B′ to E′ and B″ to F′ in our two-state averaging models.

Thus, we believe that the above models give reasonable pictures of a dynamic equilibrium which exists for ACP in solution. Such dynamic structures are obviously going to be important as we begin to examine the solution structure of proteins which lack intrachain linkages which stabilize a single structure. The methods for structure determination presented here, hopefully, take a step toward recognition of this im-

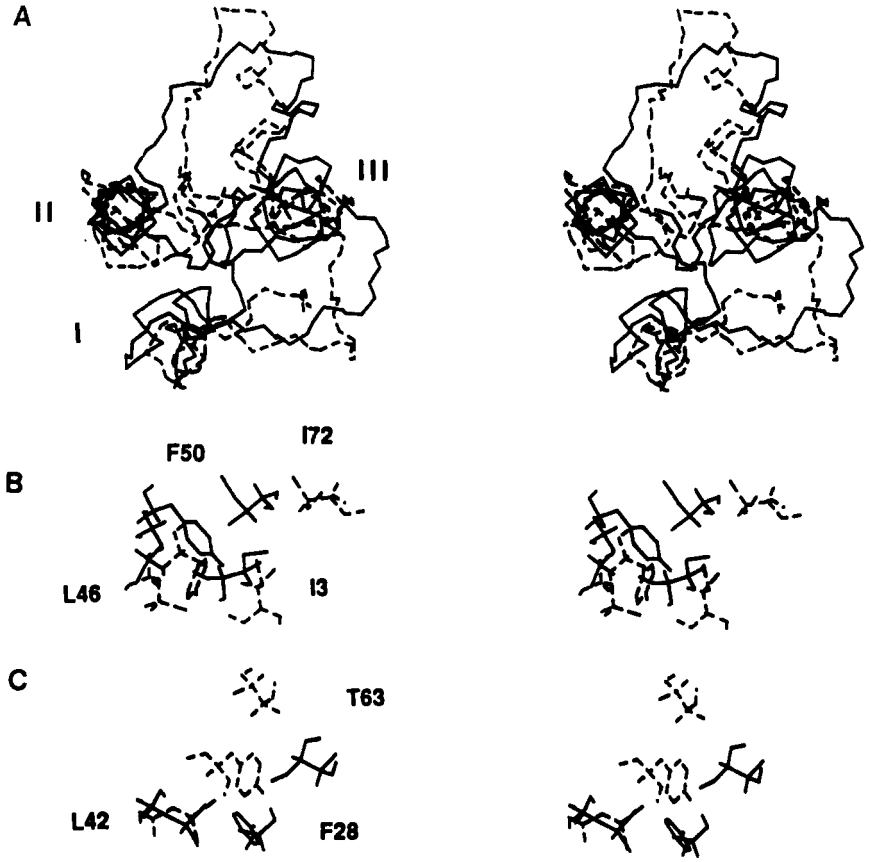

FIGURE 2: Motional averaging of the two-state model BE. Figure 2A compares the backbone structures of B′ in the BE model (solid lines) and E′ (dashed lines). Figure 2B shows details of the structures involving contacts of Phe-50 with Leu-46, Ile-3, and Ile-72. Figure 2C shows details of the structures involving contacts of Phe-28 with Leu-42 and Thr-63.

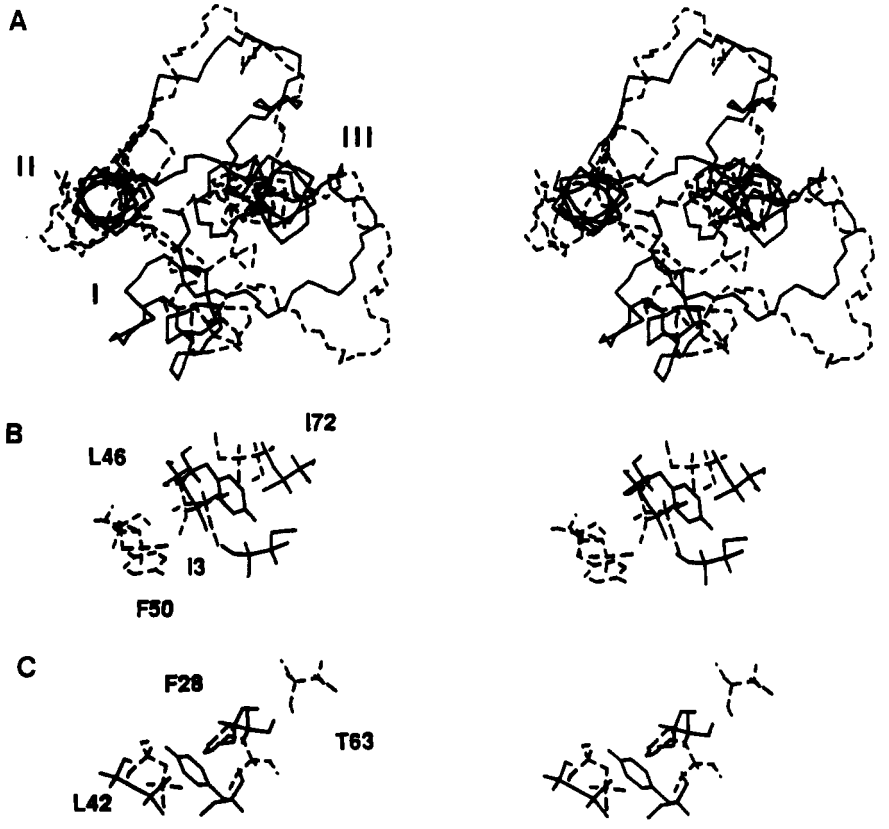

FIGURE 3: Motional averaging of the two-state model BF. Figure 3A compares the backbone structures of B″ (solid lines) and F′ (dashed lines) in the BF model. Figure 3B shows details of the structures involving contacts of Phe-50, and Figure 3C shows details of the structures involving contacts of Phe-28.

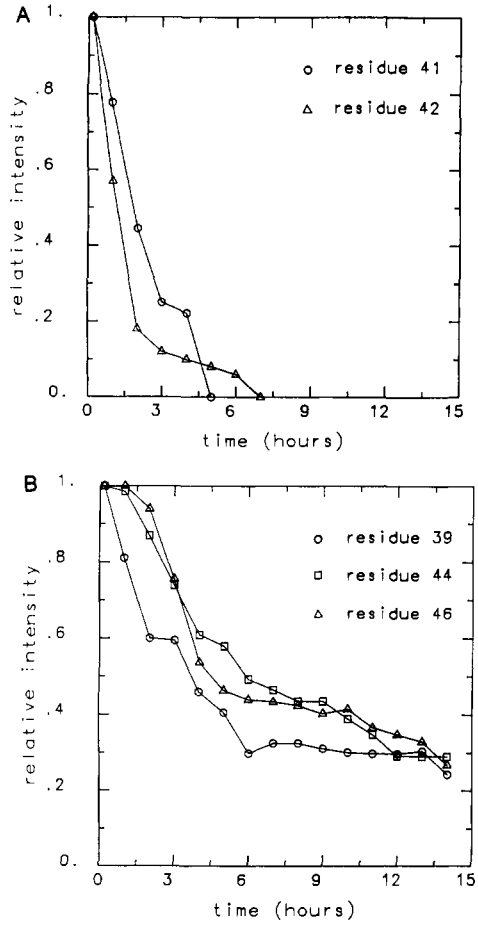

FIGURE 4: Time courses of exchange of protons for deuterium at amide sites in α-helix II. Data were acquired on an 8 mM sample of ACP prepared as described previously (Rock & Cronon, 1981)) and dissolved just before measurement in deuterated buffer at pH 5.9 in 55 mM KH_2PO_4. D_2O was added to an ACP sample, and data were acquired every 60 min for 14 h in order to see the fast exchange of amide protons with deuterium. Figure 4A shows the time courses for exchange at residues 41 and 42. Figure 4B shows the time course for exchange at residues 39, 44, and 46. Assignments and spectrometer acquisition conditions follow those of our previous study (Holak & Prestegard, 1986).

portance.

ACKNOWLEDGMENTS

We thank Dr. J. N. Scarsdale for his contributions to the development of methods for modeling dynamic equilibrium.

REFERENCES

Braun, W., & Go, N. (1985) *J. Mol. Biol. 186*, 611–626.

Braun, W., Wider, G., Lee, K. H., & Wuthrich, K. (1983) *J. Mol. Biol. 169*, 921–948.

Clore, G. M., Gronenborn, A. M., Brunger, A. T., & Karplus, M. (1985) *J. Mol. Biol. 186*, 435–455.

Clore, G. M., Brunger, A. T., Karplus, M., & Gronenborn, A. M. (1986) *J. Mol. Biol. 191*, 523–551.

Clore, G. M., Gronenborn, A. M., Nilges, M., & Ryan, C. A. (1987a) *Biochemistry 26*, 8012–8023.

Clore, G. M., Gronenborn, A. M., Nilges, M., Sukumaran, D. K., & Zarbock, J. (1987b) *EMBO J. 6*, 1833–1842.

Englander, S. W., & Kallenbach, N. R. (1983) *Q. Rev. Biophys. 16*, 521–655.

Havel, T. F., & Wuthrich, K. (1985) *J. Mol. Biol. 182*, 281–294.

Holak, T. A., & Prestegard, J. H. (1986) *Biochemistry 25*, 5766–5774.

Holak, T. A., Kearsely, S. K., Kim, Y., & Prestegard, J. H. (1988a) *Biochemistry 27*, 6135–6142.

Holak, T. A., Nilges, M., Prestegard, J. H., Gronenborn, A. M., & Clore, G. M. (1988b) *Eur. J. Biochem. 175*, 9–15.

Holak, T. A., Nilges, M., & Oschkinat, H. (1989) *FEBS Lett. 242*, 218–224.

Kay, L. E., Holak, T. A., & Prestegard, J. H. (1988) *J. Magn. Reson. 76*, 30–40.

Kline, A. D., Braun, W., & Wuthrich, K. (1988) *J. Mol. Biol. 204*, 675–724.

LeMaster, D. M., Kay, L. E., Brunger, A. T., & Prestegard, J. H. (1988) *FEBS Lett. 236*, 71–76.

Moore, J. M., Case, D. A., Chazin, W. J., Gippert, G. P., Havel, T. F., Powls, R., & Wright, P. E. (1988) *Science 240*, 314–317.

Rock, C. O., & Cronan, J. E., Jr. (1981) *Methods Enzymol. 71*, 341–351.

Scarsdale, J. N., Ram, P., Yu, R. K., & Prestegard, J. H. (1988) *J. Comput. Chem. 9*, 133–147.

Wagner, G., Stassinopoulou, C. I., & Wuthrich, K. (1984) *Eur. J. Biochem. 145*, 431–436.

Wagner, G., Braun, W., Havel, T. F., Schaumann, T., Go, N., & Wuthrich, K. (1987) *J. Mol. Biol. 196*, 611–639.